Active and Passive Elec. Comp., 2003, Vol. 26(2), pp. 95–109

Taylor & Francis
Taylor & Francis Group

SOME INVESTIGATIONS ON THE ANISOTROPY OF THE CHEMICAL ETCHING OF (h k 0) AND (h h l) SILICON PLATES IN A NaOH 35% SOLUTION. PART III: DETERMINATION OF A DATABASE FOR THE SIMULATOR TENSOSIM AND PREDICTION OF 2D ETCHING SHAPES

C. R. TELLIER[a,b]*, C. HODEBOURG[b] and T. G. LEBLOIS[a,b]

[a]*Laboratoire de Chronométrie Electronique et Piézoélectricité Ecole Nationale Supérieure de Mécanique et des Microtechniques 26 chemin de l'épitaphe, 25030 Besançon cédex, France;*
[b]*Institut des Microtechniques de Franche-Comté Avenue de l'observatoire, 25030 Besançon cédex, France*

(Received 3 September 2002; In final form 17 November 2002)

The simulation of 2D etching shapes such as surface profiles and out-of-roundness profiles related to various (h k 0) and (h h l) silicon plates or cross-sections is studied. The theoretical basis of the simulation is presented. The database for the simulator TENSOSIM is determined from a systematic analysis of experimental 2D etching shapes. Emphasis is placed on difficulties encountered in the determination procedure. Theoretical 2D etching shapes are compared with experimental shapes. A correlation between polar plots of the dissolution slowness and corresponding theoretical shapes is established. So we can conclude that the accuracy of the proposed database is sufficient for the simulation of 2D etching shapes.

Keywords: Silicon; Anisotropic etching; NaOH etchant; Tensorial and kinematic model; Simulator TENSOSIM

1 INTRODUCTION

A previous work [1, 2] on the dissolution of (h k 0) and (h h l) silicon plates in a NaOH 35% solution has given evidence for a marked anisotropy of the chemical attack. In particular, geometrical features of etched surfaces and out-of-roundness profiles were found to be orientation-dependent. These observations agree well with results [3–9] published in literature, and concerned essentially (h k 0) or (h h l) silicon plates etched in KOH, EDP or TMAH solutions. As for etchants the anisotropy for a NaOH 35% solution is of type 1 [10]. Consequently the dissolution process can be described in terms of the kinematic and tensorial model (KT model) proposed several years ago by C. R. Tellier [11–13]. In a kinematic model we search to calculate the displacement of a moving surface element of orientation (φ, θ) [12]. As soon as the displacements of all surface elements potentially present at a starting

* Corresponding author. Tel.: +33 03 81 40 28 30; E-mail: ctellier@ens2m.fr

ISSN 0882-7516 print; ISSN 1563-5031 online
DOI: 10.1080/0882751031000073869

surface are known, it becomes possible to construct numerically the final etching shape of a crystal. In the KT model the Cartesian components of the displacement vector **P** can be determined from the analytical equation for the dissolution slowness surface [12]. This possibility constitutes the major advantage of the KT model.

In this paper we propose a first set of dissolution constants to describe the anisotropy of the chemical attack of silicon crystal in a NaOH 35% solution. Various cross-sections of the proposed dissolution slowness surface are presented and discussed in terms of dissolution criteria and of conclusions [1, 2] drawn in parts I and II of this paper. Theoretical 2D etching shapes generated by the simulator TENSOSIM [10, 14–16] such as in the one hand, out-of-roundness profiles related to various (h k 0) and (h h l) cross-sections and in the other hand, various profilometry traces made on etched (h h l) and (h k 0) silicon plates are compared with experimental shapes.

2 THE KT MODEL AND THE DATABASE

2.1 The KT Model

Let us recall that in the KT model we associate at a surface element of orientation (φ, θ) (*i.e.* φ and θ are the angles of cut) a dissolution slowness vector **L** that characterises the anisotropy of the dissolution process. The vector **L** is related to parameters that can be determined experimentally in such a way [11–13] that its magnitude $L(\varphi, \theta)$ is equal to the reciprocal of the etch rate $R(\varphi, \theta)$ and that its direction coincides with that of the unit inward normal **n** to the surface element (Fig. 1a). So when the orientation of the surface element varies, the extremity of the vector **L** describes in space a representative surface called the dissolution slowness surface (Fig. 1b). The KT model constitutes a tensorial model because to express the equation $L(\varphi, \theta)$ of the dissolution slowness, we introduce dissolution constants D_o, D_i, D_{ij}, D_{ijk}, ... that can be identified as the independent constants of dissolution tensors of rank $N_R = 0, 1, 2, 3, \ldots$. So the final equation for the dissolution slowness can be written as:

$$L(\varphi, \theta) = L(n_1, n_2, n_3) = D_o + D_i n_i + D_{ij} n_i n_j + D_{ijk} n_i n_j n_k + \cdots, \quad i, j, k, \ldots = 1, 2 \text{ or } 3 \tag{1}$$

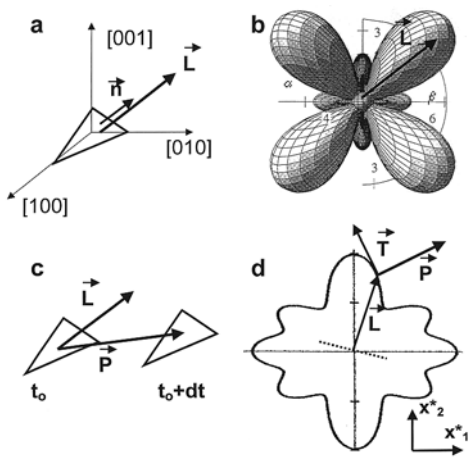

FIGURE 1 The geometry of the KT model. (a) Definition of **L**, (b) the dissolution slowness surface, (c) definition of **P**, (d) geometry for **L**, **T** and **P**.

if we take into account that the Cartesian components n_1, n_2 and n_3 of the inward normal **n** can be conveniently expressed in terms of the angles of cut (φ, θ). The number of dissolution constants is reduced by cyclic permutation of subscripts and by the symmetry that the crystal in consideration possesses [12]. Consequently, for the silicon crystal that belongs to the class m3m tensors of odd ranks vanish and the independent dissolution constants must possess even numbers of subscripts 1, 2 and 3 [13]. It is clear that in this framework the dissolution slowness surface contains the symmetry of the point group. Several works [11, 17–19] have shown that the trajectory of a surface element within the crystal during the dissolution follows a straight line so that we can associate a displacement vector **P** to the surface element (Fig. 1c). Moreover it was shown that this displacement vector lies perpendicular to the plane tangent to the dissolution slowness surface at the point of corresponding orientation. So it is possible [11] to determine the Cartesian components of **L** from Eq. (1).

When we are concerned with a 2D etching shape, we work with a particular cross-section of the dissolution slowness surface and consequently we have only to consider a polar graph $L(\beta) = F(\beta)$ of the dissolution slowness vector. The displacement **P** of the profile element lies now perpendicular to the vector **T** tangent to the polar graph (Fig. 1d) and its Cartesian components dx_1^* and dx_2^* are now, for an etching of duration dt, given by:

$$dx_1^* = \pm \frac{B(\beta)}{[F(\beta)]^2} dt \tag{2}$$

$$dx_2^* = \mp \frac{A(\beta)}{[F(\beta)]^2} dt \tag{3}$$

where β is the polar angle and where $A(\beta)$ and $B(\beta)$ are the Cartesian components of **T** in the rotated axes x_1^* and x_2^*. The choice between plus and minus signs in Eq. (2) is determined by the value of the angle that **T** makes with **L**.

2.2 The Database of the Simulator TENSOSIM

As the equation for the dissolution slowness surface involves dissolution constants that compose the database of the simulator, we have to determine the dissolution constants from experiments. An iterative procedure to extract the dissolution constants from changes in the dissolution slowness $L(\varphi, \theta)$ with orientation and from experimental etching shapes has been proposed in a previous study [20]. Care must be taken that we cannot evaluate the true dissolution slowness corresponding to a perfectly flat crystallographic surface. Effectively, we only estimate etching rates related to surfaces covered by dissolution figures that for some orientations may be markedly disorientated with respect to the reference surface (mean slopes $>10^\circ$). So a major part of the procedure is based on an analysis of etching shapes that involves two main steps. In the first step of this procedure we investigate experimental 2D etching shapes such as out-of-roundness profiles and 2D profilometry traces because:

(i) an out-of-roundness profile (ORP) related to a given cross-section (angles of cut φ_o and θ_o) constitutes a crude image [20] of the polar diagram of the dissolution slowness lying in the same section. In particular we can estimate with a sufficient accuracy ($\pm 1^\circ$) angles Ψ_M and Ψ_m for which maxima (peaks in ORP) and minima (valleys in ORP) occur in the polar graph of the dissolution slowness;

(ii) it is generally assumed that the final etching shape of a 2D surface profile made on a plate of cut (φ_o, θ_o) depends [8, 17–22] on the number and on the nature (maximum,

minimum) of the extrema in **L** present in the angular sector of the polar graph centred on the reference dissolution slowness $L(\varphi_o, \theta_o)$. So without ignoring that in the one hand, the analysis gives better conclusions when elongated dissolution figures develop on etched surfaces and that in the second hand, some artefacts can lead to false interpretations [20] it may be possible to detect minor extrema in polar graphs that cannot be distinguished on ORP.

So we encounter several difficulties in the interpretation of experimental results:

(i) the etch rate of a deeply etched surface can differ markedly from the etch rate of a crystallographic plane;
(ii) ORP furnish only the angular values of extrema in polar graphs but do not allow us to estimate the relative amplitude of successive extrema with a sufficient accuracy;
(iii) we need attention when we draw conclusions from the examination of profilometry traces.

Owing to these difficulties in the first step, several sets of dissolution constants are determined for which theoretical 2D etching shapes are derived using the simulator TENSOSIM. These theoretical shapes are compared with experimental shapes (ORP, profilometry traces). Finally the database that gives the better agreement between experiments and theory is selected. In the second step this database is used to obtain 3D theoretical shapes for membranes and mesa micromachined in differently oriented silicon plates when we start with "circular" masks. Then we again undertake a comparison between experimental and theoretical 3D etching shapes. If necessary, some slight adjustments of the dissolution constants are yet performed and we stop the iterative procedure when the selected database leads to satisfactory theoretical results. A stereographic projection of the proposed dissolution slowness surface on the (0 0 1) plane is shown in Figure 2. In addition polar graphs of **L** related to various (h k 0) and (h h l) cross-sectional planes are drawn in Figures 3 and 4 respectively. We observe that minor maxima of the dissolution slowness occur for {1 0 0} planes. Moreover the dissolution slowness surface exhibits very prolate protuberances associated with {1 1 1} planes. At this point it should be pointed out that similar features are met for various etchants [5–9]. But Figures 3 and 4 also give evidence that {1 1 0} planes are not correlated to small protuberances of the dissolution slowness surface as observed for some specific etchants such as TMAH 25% [7] and KOH 35% [8] solutions.

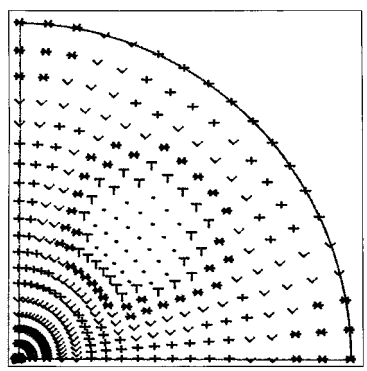

FIGURE 2 The stereographic representation of the dissolution slowness surface.

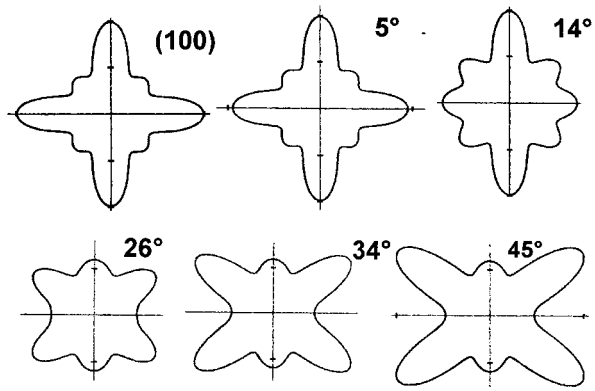

FIGURE 3 Some (h k 0) polar graphs of **L**. Values for the angle of cut φ_o are indicated on the figure. Note that for φ_o in the range [23°, 45°] the polar plot represents ln[L(φ_o, θ)] owing to the influence of the very elongated protuberances associated with {1 1 1} planes.

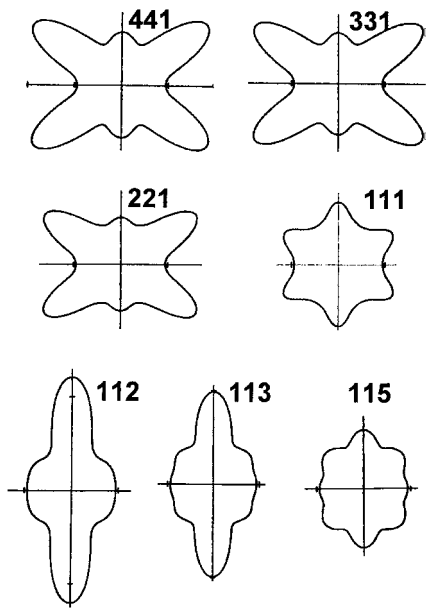

FIGURE 4 Some (h h l) polar graphs of **L** in the form ln[L(φ, θ)] as indicated on the figure. The direction ⟨1 1 0⟩ lies parallel to the horizontal axis.

3 SIMULATION OF SURFACE PROFILES

3.1 The Framework

To derive theoretical surface profiles we start either with a triangular profile composed of two elements whose slopes are $\pm\alpha_T$ ($\alpha_T = 20°$), or with the surface profile shown in Figure 5. Slopes of profile elements composing the surface profile of Figure 5 are in the range [−15°, 15°]. When we perform simulations of a 2D surface profile we work with the polar graph of the dissolution slowness **L** that is located in the cross-sectional plane containing the starting surface profile. As an example, let us examine the case of an x_3' trace placed

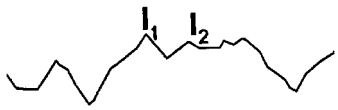

FIGURE 5 The starting surface profile related to a rough surface.

on a (h h l) plate (Fig. 6). On the polar graph we have only to consider an angular sector of $\pm\alpha_T^\circ$ centred on the dissolution slowness $\mathbf{L}_{(h\,h\,l)}$ related to the reference (h h l) surface. For an x_3' trace it is clear that as the angle of cut θ_o varies from 0° ((1 1 0) plane) to 90° ((0 0 1) plane) the dissolution slowness $\mathbf{L}_{(h\,h\,l)}$ moves on the (1 $\bar{1}$ 0) polar graph of **L**. As a consequence, etched surface profiles must exhibit progressive changes in final shape. On the contrary, to derive ⟨1 1 0⟩ traces, the simulation involves different (h′ h′ l′) polar graphs that are in cross-sections perpendicular to reference (h h l) plates. To illustrate this subject let us examine the results (Figs. 7 and 9) obtained for (1 1 5) and (3 3 1) silicon plates when we start with a triangular profile that offers the advantage of being composed of successively concave and convex intersections. In order to make the discussion more comprehensive, plots of the dissolution slowness L versus the slope α of profile elements are also given on these figures. First consider the (1 1 5) plate (Fig. 7) that lies at about 16° from the (0 0 1) plate. As noticed in a previous paper the ⟨1 1 0⟩ trace shows a mirror symmetry associated with the ($\bar{1}$ 1 0) plane. The polar graph of **L** lying in the corresponding (h′ h′ l′) plane passes through a maximum (Fig. 7A) for an orientation ($\alpha = 0^\circ$) corresponding to the reference surface, so the final etched ⟨1 1 0⟩ surface profile exhibits a symmetrical concave shape in accord with the dissolution criteria [17] stated by Irving. When the duration of etching increases, the divergence of elements trajectories causes a progressive enlargement of the curved regions. In contrast, at a starting convex intersection the trajectories of the two surface elements forming the intersection converge, making the intersection stable (*i.e.* the intersection angle *I** is conserved). So the final shape of a surface profile is primarily determined by extrema in polar graphs that induce diverging trajectories. According to dissolution criteria the presence of a **maximum** in a given polar graph of **L** related to an element of orientation α_M produces at a **concave intersection** the divergence of trajectories of elements in the vicinity of α_M. The converse situation leads to divergent trajectories at a **convex intersection**. It is just the situation that is observed if a **minimum** in a polar graph of L occurs for an element of orientation α_m. The L *vs* α plot of Fig. 7B shows a more complex situation since we are

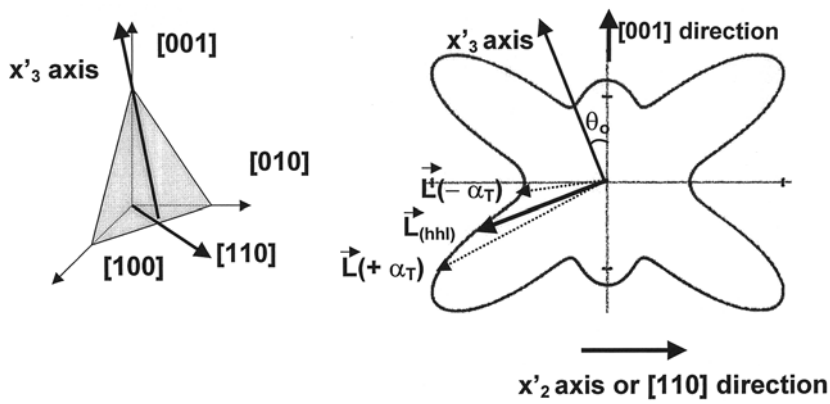

FIGURE 6 Basis of the simulation for a 2D surface profile. Here we suppose that the stylus of the mechanical profilometer moves in the direction opposite to that of the x_3' axis.

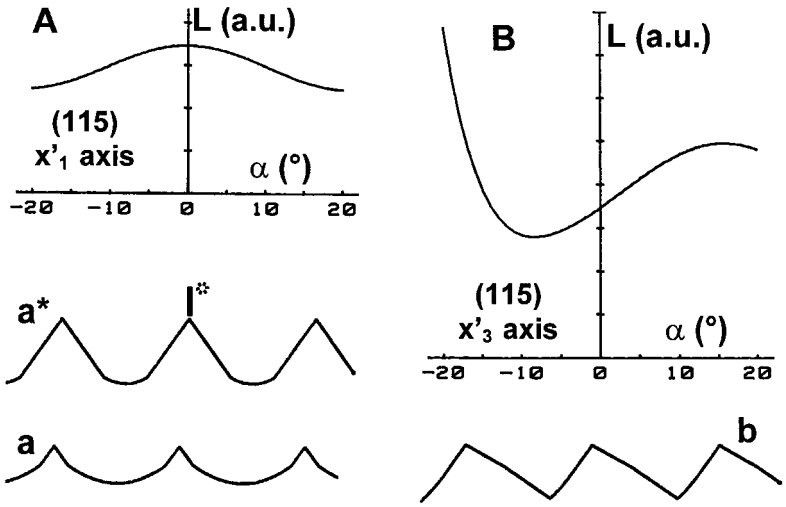

FIGURE 7 Theoretical ⟨1 1 0⟩ traces (**a**, **a***) and x_3' traces (**b**) for a 1 1 5 plate and corresponding $L(\alpha)$ plots (**A**, **B**). (**a***) and (**a**) correspond to ⟨1 1 0⟩ traces (or x_1' traces) obtained with etching times $t = 25$ a.u. and $t^* = 50$ a.u. respectively.

concerned with two successive extrema of different nature: a minimum for $\alpha_m \approx -8^\circ$ and a maximum for $\alpha_M \approx +15^\circ$. Consequently it is obvious that in terms of dissolution criteria, the simulation gives rise to a final theoretical x_3' trace with alternate concave–convex shapes and that the concave region is composed of successive more sloppiest elements. If we now turn attention to theoretical ⟨1 1 0⟩ traces made on a (3 3 1) plate (Fig. 8A, *a* and *a**) it appears that here again the polar graphs of L show a maximum for $\alpha = 0^\circ$. So a final concave background

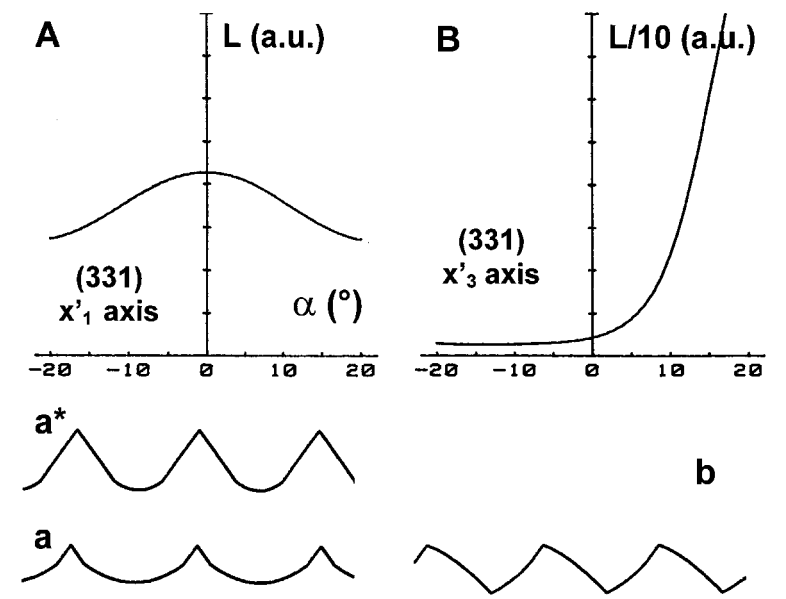

FIGURE 8 Theoretical ⟨1 1 0⟩ traces (**a**, **a***) and x_3' traces (**b**) for a 3 3 1 plate and corresponding $L(\alpha)$ plots (**A**, **B**). (**a***) and (**a**) correspond to ⟨1 1 0⟩ traces (or x_1' traces) obtained with etching times $t = 25$ a.u. and $t^* = 50$ a.u. respectively.

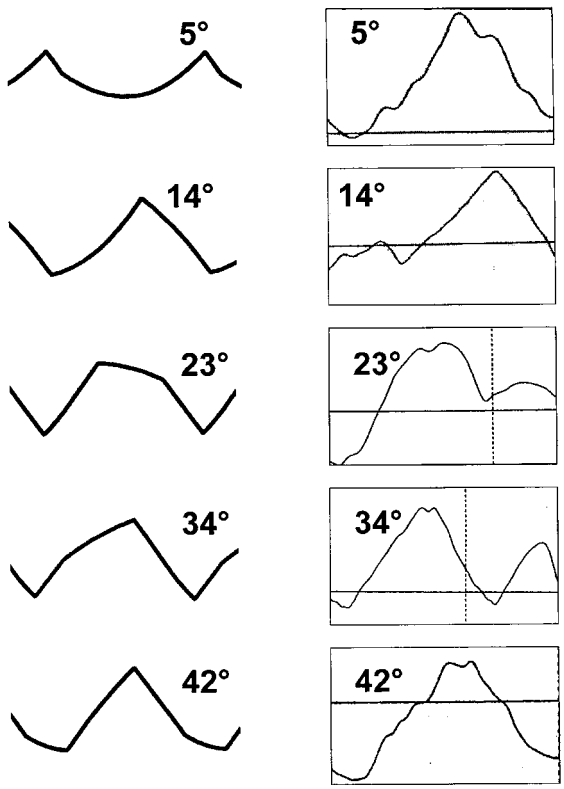

FIGURE 9 Theoretical and experimental x_1' traces for various (h k 0) plates. Values for the angle of cut φ_o are indicated on the figure.

develops in accord with experimental observations [1]. The $L(\alpha)$ plot involved in the simulation of the x_3' trace firstly presents a minimum for $\alpha_m \approx -12^\circ$, and secondly increases markedly with increasing positive slope α. In fact between 10° and 20° the $L(\alpha)$ plot possesses an inflexion point. It is clear that the changes in sign of the graph curvature produce the same effect as the presence of a maximum. Effectively it has been shown [11, 12] that the displacement vectors **P** of moving surface elements can be determined from the analytical equation of the dissolution slowness and that the calculation of the Cartesian components of **P** involves [11] partial derivatives with respect to angles that determine the orientation of elements. So even if an extremum is not really present, it may be possible to obtain curved regions associated with diverging trajectories. This situation can lead to false interpretations when we analyse experimental shapes in order to determine the dissolution slowness surface. These two examples reveal that the final shape of a surface profile is correlated to the number and the nature of extrema present on the polar graph of **L**. But care must be taken that changes in curvature (from concave to convex or vice versa) around inflexion points generate also diverging trajectories in such a way that inflexion points can act as extrema in L.

3.2 Surface Profiles for (h k 0) Plates

Let us turn attention to etched (h k 0) surfaces. Theoretical x_1' and [0 0 1] surface profiles (Figs. 9 and 10) are derived from the simulator TENSOSIM. Owing to the preceding remark it is clear that to obtain theoretical x_1' traces we use the (0 0 1) polar graph whose shape is close

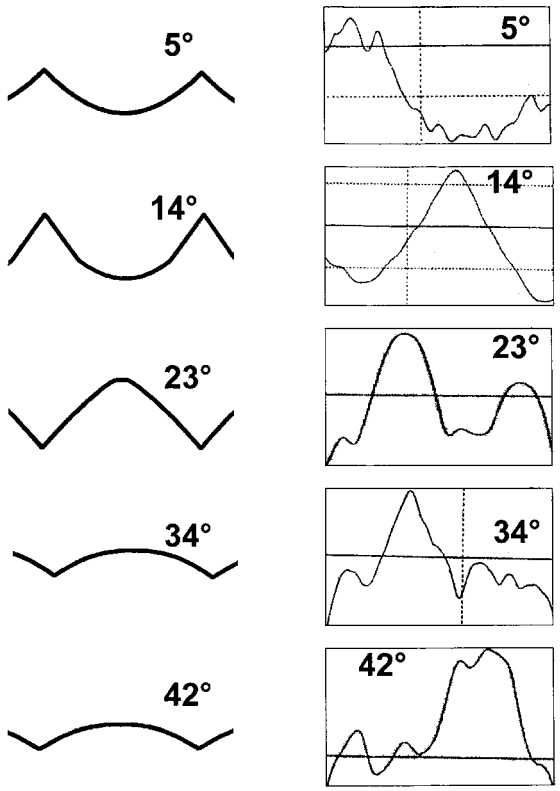

FIGURE 10 Theoretical and experimental [0 0 1] traces for various (h k 0) plates. Values for the angle of cut φ_o are indicated on the figure.

to that related to the (h k 0) section with $\varphi_o = 5^\circ$ (Fig. 3). Moreover if we take into account that the [0 0 1] axis is a fourfold axis the theoretical shape for a [0 0 1] trace can be simply derived by involving in the simulation the $[-20^\circ, +20^\circ]$ angular sector centred on the horizontal axis of the (h k 0) polar graph of **L**. When we start with a triangular profile we obtain the theoretical profiles displayed in Figures 9 and 10. The comparison of theoretical surface profiles with experimental profilometry traces shows a satisfactory agreement in particular for x_1' traces and for [0 0 1] traces related to (h k 0) plates whose angle of cut φ_o is in the range $[0^\circ, 23^\circ]$. Moreover as the angle φ_o increases from 5° to 42°, predicted x_1' surface profiles exhibit progressive changes in shape in accord with a preceding remark. So it is left as an exercise for the reader to verify that alternate concave–convex (or convex–concave) shapes are produced when minimum (maximum) and a maximum (minimum) of the polar graph of L are included in corresponding $[0^\circ, +20^\circ]$ and $[-20^\circ, 0^\circ]$ angular sectors. Moreover when **L** passes through a maximum for an orientation corresponding to the reference (h k 0) surface (angle of cut $\varphi_o = 5^\circ$ or 14°) the theoretical [0 0 1] trace is only composed of symmetrical concave portions in accord with the dissolution criteria. The converse situation that occurs for $\varphi_o = 34^\circ$ and 42° leads to the development of a convex background (Fig. 10).

3.3 Surface Profiles for (h h l) Plates

We now look at theoretical x_1' surface profiles (*i.e.* at ⟨1 1 0⟩ traces) and x_3' traces derived for various (h h l) reference surfaces using the initial surface profile of Fig. 5. This starting

surface profile constitutes a middle region, where profile elements are slightly inclined ($|\alpha| < 10^\circ$), and regions with more sloped elements. So it becomes possible to investigate the influence of initial slopes on the final shape of traces. Moreover as the slope of the various elements composing an etched surface profile decreases in amplitude with prolonged etching [21], all theoretical traces were obtained for the same duration of etching ($t = 40$ arbitrary units). As in Section 3.1 plots of the dissolution slowness L as a function of the slope α of profile elements are displayed in Figures 11 and 13. Several $\langle 1\,1\,0\rangle$ traces, correlated with the $L(\alpha)$ *vs* α plots shown in Figure 11, are drawn in Figure 12. We observe that a concave background (denoted C1) develops on any (h h l) plates because a maximum of L occurs for an orientation that coincides with that of the (h h l) reference surface. In the case of the (4 4 1) plate sloppiest elements of the initial profile contribute to convex portions (denoted C2). This behaviour is caused by the presence of two minima located symmetrically at $\pm 18^\circ$ with respect to the reference orientation, so inflexion points are present in the α range of the starting surface profile (*i.e.* in the range $[-15^\circ, +15^\circ]$). Convex portions C2 are also depicted on $\langle 1\,1\,0\rangle$ traces of (1 1 2) and (1 1 7) plates even if no minima in L are present on the corresponding plots of Figure 11. In fact the formation of these curved convex portions can be understood in terms of changes in curvatures on both sides of inflexion points, as suggested in Section 3.1. For the (2 2 1) plate we find that the theoretical $\langle 1\,1\,0\rangle$ trace exhibits a symmetrical concave background. With the preceding assumption we can for the (2 2 1) plate reasonably attribute the absence of convex portions in the $\langle 1\,1\,0\rangle$ surface profile to the fact that inflexion points are in the close vicinity of $+20^\circ$ and -20° (Fig. 11). So as the sloppiest elements disappear in the first stages of etching, a prolonged etching leads to a final concave background. The comparison of experimental shapes with theoretical shapes [1] is rather

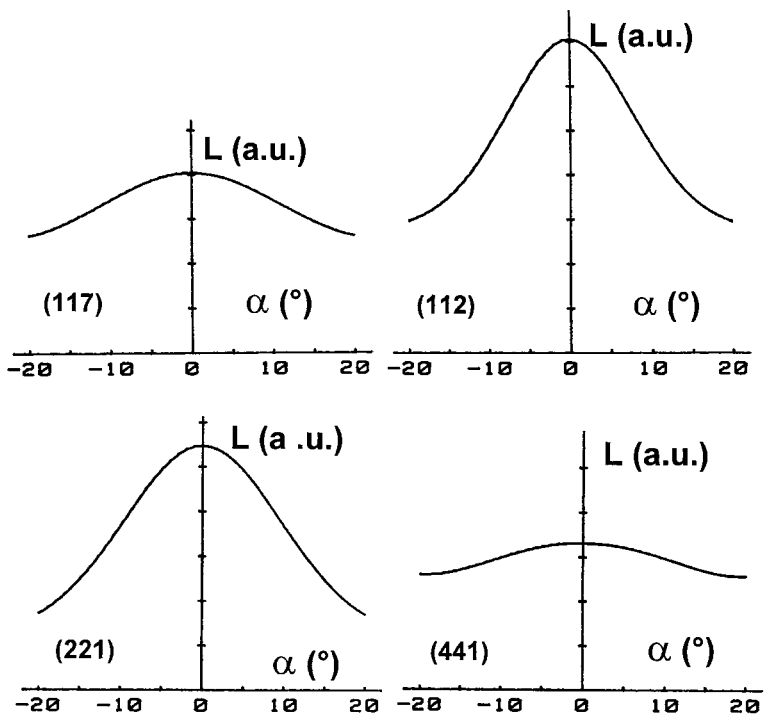

FIGURE 11 The $L(\alpha)$ plots involved in the simulation of $\langle 1\,1\,0\rangle$ traces (or x_1' traces) made on various (h h l) planes. Miller indexes are indicated on the figure.

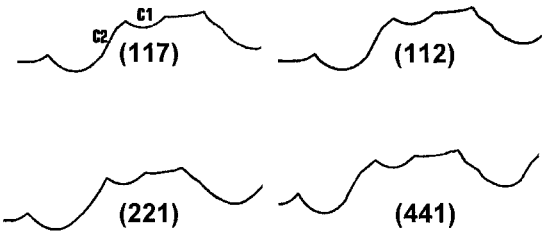

FIGURE 12 Simulation of ⟨1 1 0⟩ traces (or x_1' traces) made on various (h h l) planes. Miller indexes are indicated on the figure.

good for (1 1 7), (1 1 2) and (2 2 1) plates and less satisfactory for the (4 4 1) plate. Effectively in part I of this paper [1] we showed that ⟨1 1 0⟩ traces made on (3 3 1), (4 4 1) and (6 6 1) plates are composed of steep slopes and we qualified the characteristic shape of these ⟨1 1 0⟩ traces of "triangular".

Turning attention to the polar plots of Figure 13, we see that for x_3' traces we are concerned with more complex analyses of results. As noticed above, the simulation involves only the {1 1 0} polar plot of **L**. Figure 13 reveals that when θ_o varies from 90° to 0° the dissolution slowness passes, in the first hand, through two maxima $L_{(0\,0\,1)}$ and $L_{(1\,1\,1)}$ and, in the second hand, through two minima $L_{(1\,1\,3)}$ and $L_{(1\,1\,0)}$. To make easier the interpretation of results, it becomes essential to outline the exact role played by the successive extrema in the {1 1 0} polar plot of **L**. For this purpose the angular gaps $\Delta\alpha_m$ (for minima in the polar plot) and $\Delta\alpha_M$ (for maxima) with respect to reference orientation are listed in Table I.

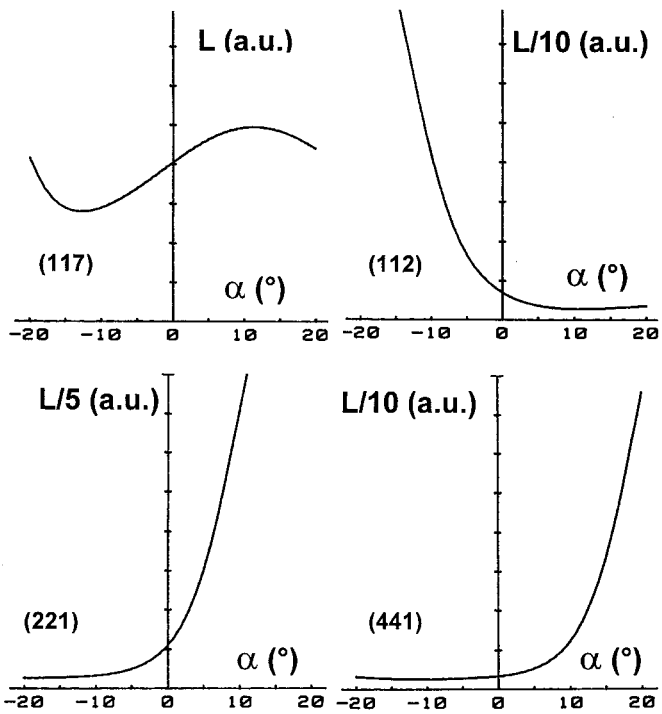

FIGURE 13 The $L(\alpha)$ plots involved in the simulation of x_3' traces made on various (h h l) planes. Miller indexes are indicated on the figure.

TABLE I Angular Gaps $\Delta\alpha_M$ and $\Delta\alpha_m$ Between the Reference Dissolution Slowness and Successive Maxima and Successive Minima in the (1 1 0) Polar Graph of **L** Respectively.

(h h l) plane	$\Delta\alpha_M$	$\Delta\alpha_m$
(1 1 7)	$\Delta\alpha_{\{1\,0\,0\}} = 11.4°$; $\Delta\alpha_{\{1\,1\,1\}} = -43.3°$	$\Delta\alpha_{\{1\,1\,3\}} = -13.9°$; $\Delta\alpha_{\{1\,1\,0\}} = -78.6°$
(1 1 2)	$\Delta\alpha_{\{1\,0\,0\}} = 35.3°$; $\Delta\alpha_{\{1\,1\,1\}} = -19.5°$	$\Delta\alpha_{\{1\,1\,3\}} = 10°$; $\Delta\alpha_{\{1\,1\,0\}} = -54.7°$
(2 2 1)	$\Delta\alpha_{\{1\,0\,0\}} = 70.5°$; $\Delta\alpha_{\{1\,1\,1\}} = 15.8°$	$\Delta\alpha_{\{1\,1\,3\}} = 35.3°$; $\Delta\alpha_{\{1\,1\,0\}} = -19.5°$
(4 4 1)	$\Delta\alpha_{\{1\,0\,0\}} = 80°$; $\Delta\alpha_{\{1\,1\,1\}} = 25.3°$	$\Delta\alpha_{\{1\,1\,3\}} = 54.7°$; $\Delta\alpha_{\{1\,1\,0\}} = -10°$

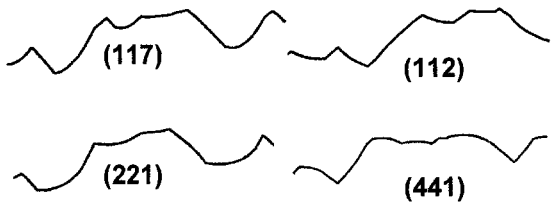

FIGURE 14 Simulation of x_3' traces made on various (h h l) planes. Miller indexes are indicated on the figure.

The theoretical shape of the x_3' trace (Fig. 14) can be for the (1 1 7) plate explained in terms of a maximum and a minimum of L present in the $[-15°, +15°]$ range. For (2 2 1) and (4 4 1) plates, the simulation generates concave–convex x_3' profiles. Differences between the two profiles displayed in Figure 14 concern only the middle region. This region appears to be composed of concave elements with positive slope for the (2 2 1) plate, and of convex elements with negative slope in the case of the (4 4 1) plate. In fact the change of curvature from concave (for the minimum $L_{(1\,1\,0)}$) to convex (for the maximum $L_{(1\,1\,1)}$) in the polar plot occurs for the (2 2 1) plate around $\alpha = 0°$ but for positive slopes causing a concavity of profile elements with positive slope in the middle region. It is equivalent to say that the influence of the very accentuated maximum $L_{(1\,1\,1)}$ is predominant for profile elements with positive slopes. As for the (4 4 1) plate, the maximum $L_{(1\,1\,1)}$ is rejected relatively far from the $[-15°, +15°]$ range. The influence of the minimum $L_{(1\,1\,0)}$ now covers elements with small negative slopes. It is the reason that the middle region is composed of curved convex elements with negative slopes. If we now examine the theoretical x_3' trace related to the (1 1 2) plate, we meet a situation converse to the (2 2 1) plate behaviour. Consequently, as expected, the final x_3' profile is formed of curved convex portions for higher slopes and of concave elements with negative slopes particularly in the middle region.

This discussion outlines the difficulties we encounter when we try to analyse experimental traces in terms of extrema in the polar diagrams of the dissolution slowness. Nevertheless it should be mentioned that the comparison of experimental x_3' traces with theoretical predictions is satisfactory. Effectively in a previous work [1] we obtained alternate convex–concave shapes for (h h l) plates with θ_o in ranges $[6°, 36°]$ and $[36°, 81°]$. Since in profilometry measurements we cannot control the positive direction of x_3' axis, no further conclusion can be made on the agreement between theory and experiments.

4 SIMULATION OF ORP

When we perform simulations of etched ORP we assume that the starting cross-section of a cylindrical crystal is composed of successive linear segments formed by intersecting planes that are tangent to the starting circular section. Consequently, the knowledge of the entire

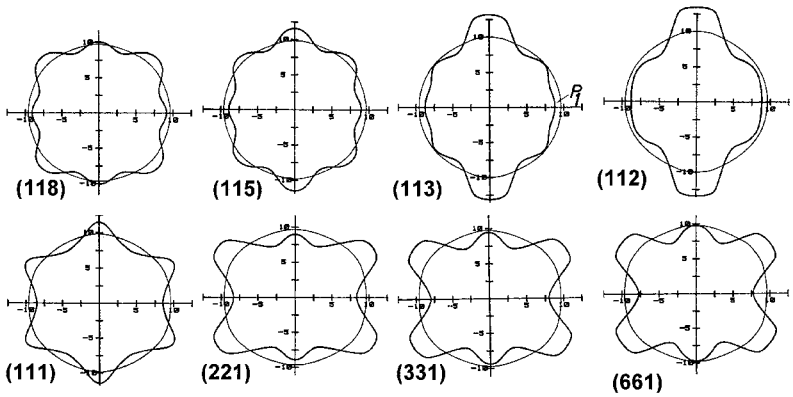

FIGURE 15 Theoretical out-of-roundness profiles for various (h h l) cross-sectional planes as indicated on the figure. Note that theoretical ORP are rotated 90° with respect to experimental ORP [1].

polar graph of **L** lying in the cross-sectional plane enables us to derive simulation of the etched cross-section and of ORP. It follows that we are now concerned with the largest angular sector (*i.e.* 0° to 360°). So the etched cross-section is found to involve only profile elements whose dissolution slowness remains in the close vicinity of minima L_m in the cross-sectional polar graph of **L**. Effectively at this point it is of interest to recall that in terms of dissolution criteria [17, 21], the etching shape of a starting 2D convex profile must be primarily determined by minima in the corresponding polar diagram of **L**. Moreover, peaky minima that make trajectories of profile elements markedly diverging yield crudely linear portions of etched cross-sections, whereas smooth minima produce curved portions. Figure 15 shows ORP related to various (h h l) cross-sectional planes. Examination of these ORP reveals several features.

(i) As expected, theoretical ORP exhibit progressive changes in etching shapes when the angle of cut θ_o increases from 0° to 90°.
(ii) Theoretical etching shapes of ORP agree well with experimental shapes [1] even if in Figure 14 of part I [1] the experimental ORP are rotated by about 90° with respect to the theoretical ORP of Figure 15.
(iii) Comparison of theoretical ORP (Fig. 15) with the polar diagrams of Figure 4 shows that in fact (h h l) ORP resemble corresponding polar graphs of **L**. Consequently, an experimental ORP allows us to evaluate with a sufficient accuracy orientations (φ_m, θ_m) of planes associated with minima in the polar graph.

Taking into account the feature (iii) it appears that a comparison of experimental ORP related to etched (h k 0) sections with the polar plots of Figure 3 enables us to verify rapidly the adequacy of simulated (h k 0) ORP with experimental ones [1].

5 DISCUSSION AND CONCLUSION

Section 3 gives evidence for some deviations between experimental traces and theoretical surface profiles. Let us discuss the origin of such deviations. Firstly for (h k 0) cuts close to the (1 1 0) plate, the agreement between theoretical and experimental x_1' and [0 0 1] surface profiles is not so good as that observed for cuts in the range $\varphi_o < 30°$. This deviating behaviour is certainly due to the development on etched plates of dissolution figures [1] whose

characteristic shape crudely resembles a pyramidal shape. So for these cuts we are far from the ideal case for the simulation of 2D surface profiles. That is to say, we are far from dissolution figures elongated along a preferential direction that lies perpendicular to the direction of profilometry trace. This interpretation can be also retained to understand the differences between theoretical and experimental traces observed for (3 3 1), (4 4 1) and (6 6 1) plates. Moreover, for other plates it is possible to correlate polar graphs of L to experimental traces. So if we consider the results obtained for profilometry traces, the proposed database seems to be rather satisfactory. Using this database to derive (h k 0) and (h h l) ORP from the simulator TENSOSIM gives theoretical shapes in close accord with experimental ORP. It should be pointed out that all valleys and peaks depicted on experimental ORP are present on theoretical ORP. In particular the small peak P_1 that the (1 1 3) ORP possesses in theory (Fig. 15) disappears on the (1 1 2) ORP in complete agreement with experimental observations.

Consequently, this study enables us to draw two conclusions.

(i) The dissolution process is conveniently described in terms of a kinematic and tensorial model for the anisotropic dissolution.
(ii) At first sight, the adequacy of the proposed dissolution slowness surface is good.

However, this study also places emphasis on limitations in the analysis of 2D etching shapes. In particular we outline that it is very difficult to extract the amplitude of successive valleys and protuberances of the dissolution slowness surface from experimental 2D etching shapes. A method to overcome this difficulty consists of comparing theoretical 3D etching shapes with experimental ones. Effectively we can reasonably expect that lateral extents of quasi-planar or of curved facets limiting a 3D shape depend on the relative amplitude of successive extrema. So results on the simulation of 3D structures micromachined in (h h l) silicon plates will be reported in a future paper.

References

[1] Hodebourg, C. and Tellier, C. R. (2001). Some investigations on the anisotropy of the chemical etching of (h k 0) and (h h l) silicon plates in a NaOH 35% solution. Part I: 2D etching shapes, *Active and Passive Elec. Comp.*, **24**, 31–56.
[2] Tellier, C. R., Hodebourg, C. and Durand, S. (2001). Some investigations on the anisotropy of the chemical etching of (h k 0) and (h h l) silicon plates in a NaOH 35% solution. Part II: 3D etching shapes, analysis and comparison with KOH 56%. *Active and Passive Elec. Comp.*, **24**, 243–264.
[3] Van Veenendaal, E., Sato, K., Shikida, M., Nijdam, A. J. and Van Suchtelen, J. (2001). Micromorphology of single crystalline silicon surfaces during anisotropic wet chemical etching in KOH: Velocity source forests. *Sensors and Actuators A*, **93**, 232–242.
[4] Van Veenendaal, E., Sato, K., Shikida, M. and Van Suchtelen, J. (2001). Micromorphology of single crystalline silicon surfaces during anisotropic wet chemical etching in KOH and TMAH. *Sensors and Actuators A*, **93**, 219–231.
[5] Schnakenberg, U., Benecke, W. and Lochel, B. (1990). NH_4OH-based etchants for silicon micromachining. *Sensors and Actuators A*, **21–23**, 1031–1035.
[6] Barycka, I. and Zubel, I. (1995). Silicon anisotropic etching in KOH-isopropanol etchant. *Sensors and Actuators A*, **48**, 229–238.
[7] Charbonnieras, A. R. and Tellier, C. R. (1999). Characterization of the anisotropic chemical attack of {h k 0} silicon plates in a TMAH solution. Determination of a database. *Sensors and Actuators A*, **77**, 81–97.
[8] Brahim-Bounab, A. and Tellier, C. R. (1994). Anisotropic etching of silicon crystals in KOH solutions. Part 1: Experimental etched shapes and determination of the dissolution slowness surface. *J. Mater. Sci.*, **29**, 5971–5993.
[9] Tellier, C. R., Leblois, T. G. and Charbonnieras, A. (2000). Chemical etching of {h k 0} silicon plates in EDP. Part 1: Experiments and comparison with TMAH. *Active and Passive Elec. Comp.*, **23**, 243–264.
[10] Tellier, C. R., Hodebourg, C. and Leblois, T. G. (2002). Simulation of 3D shapes etched in a 35% NaOH solution. *CIMTEC 2002 and 3rd Forum on New Materials*, 14–18 July, Florence (to be published.)
[11] Tellier, C. R. (1989). A three-dimensional kinematic model for the dissolution of crystals. *J. Cryst. Growth*, **96**, 450–452.

[12] Tellier, C. R. (1988). Micro-usinage Chimique du Quartz: Modélisation et Contrôle par Microscopie Electronique à Balayage. *Rapport DRET, Convention 85.34.099.470.75.01*, 169 pp.
[13] Brahim-Bounab, A., Amaudrut, J. Y. and Tellier, C. R. (1991). The dissolution slowness of cubic crystals: Part I. Theoretical and three-dimensional representation for class 23. *J. Mater. Sci.*, **26**, 5585–5594.
[14] Tellier, C. R. (1998). Anisotropic etching of silicon crystals in KOH solution. Part III. Experimental and theoretical shapes for 3D structures micromachined in (h k 0) plates. *J. Mater. Sci.*, **33**, 117–131.
[15] Tellier, C. R. and Durand, S. (1997). Micromachining of (h h l) structures: Experiments and 3D simulation of etched shapes. *Sensors and Actuators A*, **60**, 168–175.
[16] Tellier, C. R., Charbonnieras, A. and Hodebourg, C. (2001). Simulation of etching shapes for {h h l} structures micromachined in a TMAH 25% solution. *Sensor 2001*, May 8–10, 2001, Nuremberg, Germany, AMA Service GmbH Publisher, pp. 269–274.
[17] Irving, B. A. (1962). In: Holmes, P. J. (Ed.), *The Electrochemistry of Semiconductors.* Academic Press, London, pp. 262–294.
[18] Frank, F. C. (1965). In: Doremus, R. H., Robert, B. W. and Turnbull, D. (Eds.), *Growth and Perfection of Crystals.* Wiley, New York, pp. 411–417.
[19] Sangwal, K. (1987). *Etching of Crystals.* North-Holland, Amsterdam.
[20] Leblois, T. G. and Tellier, C. R. (1992). Determination of the dissolution slowness surface by study of etched shapes. Morphology of the dissolution slowness surface and theoretical etched shapes. *J. Phys. III France*, **2**, 1259–1286.
[21] Tellier, C. R., Amaudrut, J. Y. and Brahim-Bounab, A. (1991). The dissolution slowness of cubic crystals: Part II: Applications to class 23 and to combined etching and lithography techniques. *J. Mater. Sci.*, **26**, 5595–5607.
[22] Tellier, C. R. and Brahim-Bounab, A. (1994). Anisotropic etching of silicon crystals in KOH solutions. Part 2: Theoretical two-dimensional etched shapes: Discussion of the adequation of the dissolution slowness surface. *J. Mater. Sci.*, **29**, 6354–6378.